AAS 22-564

ROBUST TRAJECTORY OPTIMIZATION AND GN&C PERFORMANCE ANALYSIS FOR NRHO RENDEZVOUS

David Woffinden[*], Simon Shuster[†], David Geller[‡], Stefan Bieniawski [§]

This paper evaluates several candidate Near-Rectilinear Halo Orbits (NRHO) rendezvous trajectory designs using linear covariance (LinCov) analysis and determines the optimal locations for NRHO rendezvous translational burn locations. The performance of several candidate relative trajectory designs are determined as a function of relative navigation accuracy (angles only), inertial optical navigation (OpNav), range observability maneuvers, maneuver execution errors, targeting logic, and environment uncertainties. Some key elements of this analysis include relative navigation performance in an NRHO, relative trajectory dispersion performance, and total 3-sigma delta-v performance. This development provides the motivation and insight to then determine an optimal and robust end-to-end NRHO rendezvous trajectory, including the determination of the optimal locations of each translational burn and the best optical navigation targets to track. The strategy utilizes a LinCov simulation and a genetic optimization algorithm (GA) to analyze a complete end-to-end optimal NRHO rendezvous trajectory design that is robust to navigation errors, maneuver execution errors, and environment uncertainties.

INTRODUCTION

Integral to the NASA programs that are pushing for lunar exploration and beyond, as evident with the Orion and Gateway[1] programs, is the execution of rendezvous, proximity operations, and docking (RPOD) in an Earth-Moon Near Rectilinear Halo Orbit (NRHO).[2,3] The NRHO trajectories maintained by Gateway are a subset of the halo orbit families and is characterized by a close passage over one of the lunar poles. As depicted in Figure 1, the NRHO proposed for future Gateway missions is a southern NRHO which reaches the furthest distance from the Moon over the lunar south pole. The period of this particular NRHO is approximately seven days. The vision for Gateway is a crew-tended cislunar haven that would be used as a staging point for both robotic and crewed lunar surface missions and for enabling travel to Mars. The plans to assemble the Gateway orbiting outpost requires the delivery of multiple modules and elements, each requiring RPOD activities. Although the ability to successfully perform RPOD has been the cornerstone of human space exploration since its inception, the new flight regime in an NRHO poses unique challenges.

This work begins investigating the process to optimize rendezvous trajectory profiles in an NRHO that account for the complex interaction of the overall integrated guidance, navigation, and control (GN&C) system performance while minimizing the relative trajectory dispersions and total 3-sigma delta-v usage. Relative navigation accuracy, inertial navigation errors, translational burn placement,

[*]Aerospace Engineer, GN&C Autonomous Flight Systems Branch, NASA Johnson Space Center, Houston TX, 77058
[†]GN&C Engineer, Space Dynamics Laboratory, North Logan, UT, 84341
[‡]Professor, Mechanical and Aerospace Engineering Department, Utah State University, Logan, UT 84322
[§]Principal Technologist for Autonomy GN&C, Blue Origin LLC, Renton, WA, 98057.

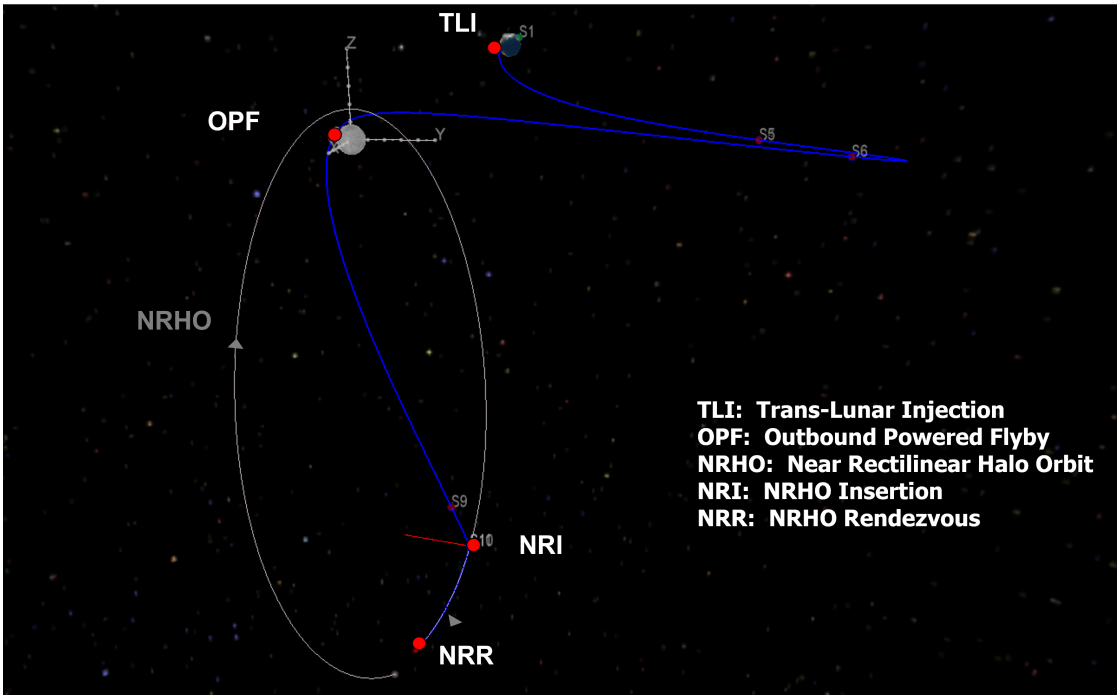

Figure 1. Earth Outbound Trajectory to a Southern Near Rectilinear Halo Orbit (NRHO).

maneuver execution errors, relative targeting algorithms, disturbance accelerations acting on both vehicles, and initial state uncertainties are all integrated into the optimization process. The inclusion of the system uncertainty in the trajectory design process is referred to as robust trajectory optimization or robust trajectory design. Previous work has developed and demonstrated this optimization strategy for rendezvous in low Earth orbit.[4] It was then extended to cis-lunar outbound trajectories to an NRHO.[5] Currently, these robust trajectory optimization principles are being applied to solve lunar powered descent and landing[6] along with Mars aerocapture[7] problems.

The objective of this research is to demonstrate robust trajectory optimization for an end-to-end scenario from low Earth orbit (LEO) through the initial phases of an NRHO rendezvous where both inertial and relative navigation are key driving factors. For this study, no radiometric tracking from the ground is assumed such that only optical cameras are utilized as the primary navigation source. To highlight the sensitivity of the integrated GN&C performance to the proposed relative motion profiles along with the selected relative navigation system, two notional rendezvous trajectories are evaluated with each having two variations where different translational burn locations and times are adopted. These range-observability maneuvers are evaluated for their robustness to uncertainties, errors, and total trajectory correction delta-v performance. The final step choses one of the profiles and then utilizes linear covariance (LinCov) analysis techniques combined with a genetic algorithm (GA) to identify a complete end-to-end optimal NRHO trajectory design that is robust to navigation errors, maneuver execution errors, and environment uncertainties. Both the cis-lunar outbound trajectory along with the relative rendezvous trajectory correction burns are optimally located to reduce trajectory dispersions and total delta-v usage.

To develop and demonstrate these core concepts and capabilities for robust trajectory optimization and analysis for NRHO rendezvous, the first section of the paper outlines the analysis approach

by defining the performance metrics, linear covariance analysis techniques, and the optimization problem formulation. The next major section provides an overview of the trajectory designs, relative navigation sensors, and initial trade study results highlighting the sensitivity of performance between the selected trajectory design and sensor suite selected. Given these general insights, the optimal end-to-end performance is derived by applying the rendezvous robust trajectory optimization analysis with different objective functions to determine the best trajectory correction burn placement and optical sensor tracking strategy. The final section concludes with summarizing key trends and design recommendations moving forward.

ANALYSIS APPROACH

Performance Metrics

To analyze the performance of several candidate NRHO rendezvous trajectory designs and identify optimal conditions, there are several performance metrics that are utilized which include the true trajectory dispersions $\delta\mathbf{x}$, the navigation dispersions $\delta\hat{\mathbf{x}}$, the true navigation error $\delta\mathbf{e}$, and the onboard navigation error $\delta\hat{\mathbf{e}}$ as depicted in Figure 2. The true dispersions $\delta\mathbf{x}$ are defined as the

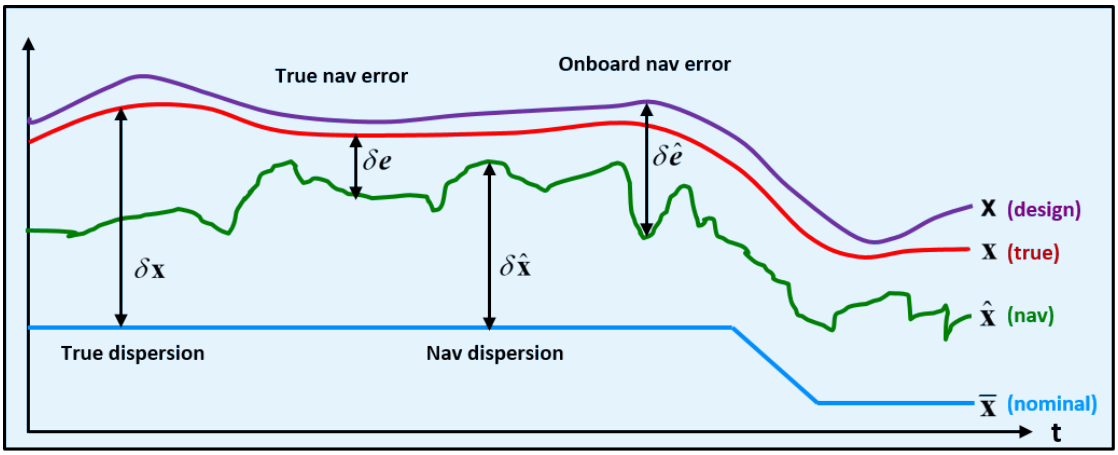

Figure 2. GN&C Performance Metric Variables

difference between the true state $\mathbf{x}$ and the nominal state $\bar{\mathbf{x}}$. The true state $\mathbf{x}$ is an n-dimensional vector that represents the *real world* environment or actual state.

$$\delta\mathbf{x} \triangleq \mathbf{x} - \bar{\mathbf{x}} \qquad \mathbf{D} = E\left[\delta\mathbf{x}\delta\mathbf{x}^{\mathrm{T}}\right] \tag{1}$$

The nominal state $\bar{\mathbf{x}}$ is also an n-dimensional vector that represents the desired or reference state. The covariance of the environment dispersions, $\mathbf{D}$, indicates how precisely the system can follow a desired trajectory.

The navigation dispersions $\delta\hat{\mathbf{x}}$ are defined as the difference between the navigation state $\hat{\mathbf{x}}$ and the nominal state $\bar{\mathbf{x}}$. The navigation state is an $\hat{n}$-dimensional vector ($\hat{n} < n$) that represents the filter's estimated state.

$$\delta\hat{\mathbf{x}} \triangleq \hat{\mathbf{x}} - \mathbf{M}_x\bar{\mathbf{x}} \qquad \hat{\mathbf{D}} = E\left[\delta\hat{\mathbf{x}}\delta\hat{\mathbf{x}}^{\mathrm{T}}\right] \tag{2}$$

The matrix $\mathbf{M}_x$ is an $(\hat{n} \times n)$ matrix that maps the estimated state in terms of the true and nominal state. The covariance of the navigation dispersions, $\hat{\mathbf{D}}$, reflect how precisely the onboard system thinks it can follow a prescribed reference trajectory.

The true navigation error $\delta\mathbf{e}$ is the difference between the environment and navigation states. It is also the difference between the environment and the navigation dispersions.

$$\delta\mathbf{e} \stackrel{\Delta}{=} \mathbf{M}_x\mathbf{x} - \hat{\mathbf{x}} = \mathbf{M}_x\delta\mathbf{x} - \delta\hat{\mathbf{x}} \qquad\qquad \mathbf{P} = E\left[\delta\mathbf{e}\delta\mathbf{e}^{\mathrm{T}}\right] \tag{3}$$

The covariance of the true navigation error, $\mathbf{P}$, quantifies how precisely the onboard navigation system can estimate the actual state.

The onboard navigation error $\delta\hat{\mathbf{e}}$ itself is never computed, but it is used to develop the onboard navigation filter equations. It is defined as the difference between the design state, x, and the navigation state $\hat{\mathbf{x}}$.

$$\delta\hat{\mathbf{e}} \stackrel{\Delta}{=} \mathrm{x} - \hat{\mathbf{x}} \qquad\qquad \hat{\mathbf{P}} = E\left[\delta\hat{\mathbf{e}}\delta\hat{\mathbf{e}}^{\mathrm{T}}\right] \tag{4}$$

The covariance of the onboard navigation error, $\hat{\mathbf{P}}$, quantifies how precisely the onboard navigation system expects it can determine the actual state. The performance of the onboard navigation system is determined by comparing $\hat{\mathbf{P}}$ to the actual navigation performance $\mathbf{P}$. If the *true* states and the *design* states are assumed to be the same, then the true navigation covariance will equal the onboard navigation covariance.

The covariances of the true dispersions, navigation dispersions, true navigation error, and the onboard navigation error are ultimately used to analyze and assess the performance of a proposed GN&C system. A common approach to obtain these performance metrics is to use a Monte Carlo simulation outlined in Figure 3, where the sample statistics of hundreds or thousands of runs, N, are used to numerically compute the desired covariance matrices.

$$\mathbf{D} = \frac{1}{N-1}\sum \delta\mathbf{x}\delta\mathbf{x}^{\mathrm{T}} \qquad \hat{\mathbf{D}} = \frac{1}{N-1}\sum \delta\hat{\mathbf{x}}\delta\hat{\mathbf{x}}^{\mathrm{T}} \qquad \mathbf{P} = \frac{1}{N-1}\sum \delta\mathbf{e}\delta\mathbf{e}^{\mathrm{T}} \tag{5}$$

The onboard navigation error covariance $\hat{\mathbf{P}}$ is the navigation filter covariance for each run. This same statistical information can be obtained using linear covariance analysis techniques.

Linear covariance analysis incorporates the non-linear system dynamics models and GN&C algorithms to generate a nominal reference trajectory $\bar{\mathbf{x}}$ which is then used to propagate, update, and correct an onboard navigation covariance matrix $\hat{\mathbf{P}}$ and an augmented state covariance matrix $\mathbf{C}$,

$$\mathbf{C} = E\left[\delta\mathbf{X}\delta\mathbf{X}^{\mathrm{T}}\right] \tag{6}$$

where the augmented state $\delta\mathbf{X}^{\mathrm{T}} = [\delta\mathbf{x}^{\mathrm{T}}\ \delta\hat{\mathbf{x}}^{\mathrm{T}}]$ consists of the true dispersions and the navigation dispersions. Pre- and post-multiplying the augmented state covariance matrix by the following mapping matrices, the covariances for the trajectory dispersions, navigation dispersions, and the navigation error can be obtained.

$$\begin{aligned}
\mathbf{D} &= [\,\mathbf{I}_{n\times n},\ \mathbf{0}_{n\times\hat{n}}\,]\,\mathbf{C}\,[\,\mathbf{I}_{n\times n},\ \mathbf{0}_{n\times\hat{n}}\,]^{\mathrm{T}} \\
\hat{\mathbf{D}} &= [\,\mathbf{0}_{\hat{n}\times n},\ \mathbf{I}_{\hat{n}\times\hat{n}}\,]\,\mathbf{C}\,[\,\mathbf{0}_{\hat{n}\times n},\ \mathbf{I}_{\hat{n}\times\hat{n}}\,]^{\mathrm{T}} \\
\mathbf{P} &= [\,\mathbf{I}_{\hat{n}\times n},\ -\mathbf{I}_{\hat{n}\times\hat{n}}\,]\,\mathbf{C}\,[\,\mathbf{I}_{\hat{n}\times n},\ -\mathbf{I}_{\hat{n}\times\hat{n}}\,]^{\mathrm{T}}
\end{aligned} \tag{7}$$

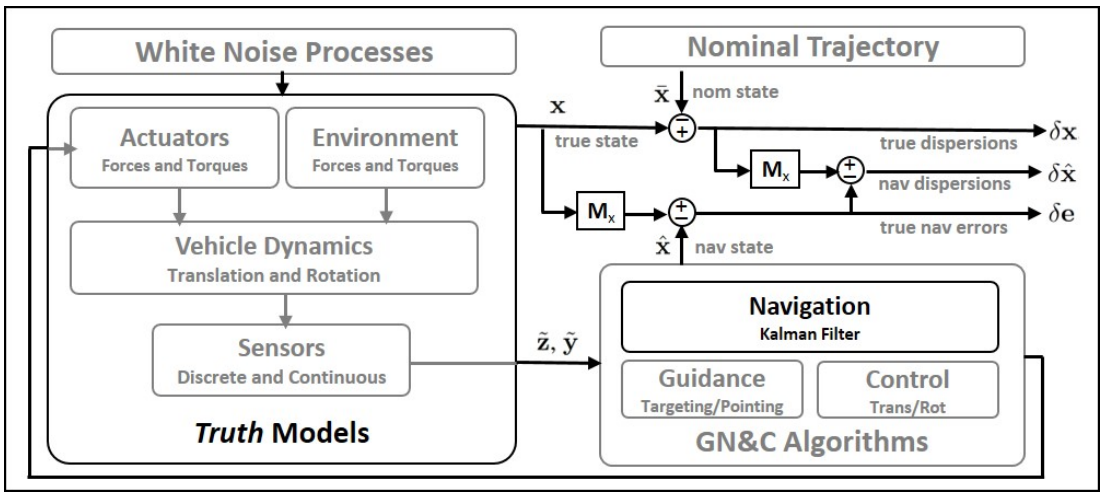

Figure 3. Extracting GN&C Performance Metrics Using Monte Carlo Techniques

Linear Covariance Analysis

The linear covariance analysis equations used to propagate, update, and correct both the augmented state covariance matrix and the onboard navigation covariance matrix are summarized here along with the LinCov analysis inputs. For additional details regarding the development and implementation of the linear covariance simulation, see the following references.[8, 9, 10, 11, 12, 13]

LinCov Analysis Modeling The discrete-time propagation equations for augmented state covariance matrix $\mathbf{C}$ and the onboard navigation covariance matrix $\hat{\mathbf{P}}$ are

$$\mathbf{C}(t_{k+1}) = \mathbf{\Phi}(t_{k+1}, t_k)\mathbf{C}(t_k)\mathbf{\Phi}^T(t_{k+1}, t_k) + \mathbf{G}\mathbf{Q}\mathbf{G}^T \tag{8}$$

$$\hat{\mathbf{P}}(t_{k+1}) = \hat{\mathbf{\Phi}}(t_{k+1}, t_k)\hat{\mathbf{P}}(t_k)\hat{\mathbf{\Phi}}^T(t_{k+1}, t_k) + \hat{\mathbf{G}}\hat{\mathbf{Q}}\hat{\mathbf{G}}^T \tag{9}$$

where $\mathbf{\Phi}$ and $\hat{\mathbf{\Phi}}$ are augmented and onboard state transition matrices respectively for the linearized perturbation dynamics about the reference trajectory. The mapping matrices, $\mathbf{G}$ and $\hat{\mathbf{G}}$, are used to map environmental and navigation process noise characterized by $\mathbf{Q}$ and $\hat{\mathbf{Q}}$, into $\mathbf{C}$ and $\hat{\mathbf{P}}$.

The measurement update equations for augmented and navigation state covariance matrices, $\mathbf{C}$ and $\hat{\mathbf{P}}$, at a measurement time t_i are

$$\mathbf{C}^+(t_i) = \mathbf{A}\mathbf{C}^-(t_i)\mathbf{A}^T + \mathbf{B}\mathbf{R}^j(t_i)\mathbf{B}^T \tag{10}$$

$$\hat{\mathbf{P}}^+(t_i) = \left[\hat{\mathbf{I}} - \hat{\mathbf{K}}^j(t_i)\hat{\mathbf{H}}^j\right]\hat{\mathbf{P}}^-(t_i)\left[I - \hat{\mathbf{K}}^j(t_i)\hat{\mathbf{H}}^j\right]^T + \hat{\mathbf{K}}^j(t_i)\hat{\mathbf{R}}^j(t_i)\hat{\mathbf{K}}^j(t_i)^T \tag{11}$$

where the superscript 'j' denotes the jth measurement type. The Kalman gain is written as

$$\hat{\mathbf{K}}^j(t_i) = \hat{\mathbf{P}}(t_i)(\hat{\mathbf{H}}^j)^T\left[\hat{\mathbf{H}}^j\hat{\mathbf{P}}^-(t_i)(\hat{\mathbf{H}}^j)^T + \hat{\mathbf{R}}^j(t_i)\right]^{-1} \tag{12}$$

The matrices $\hat{\mathbf{H}}$ and $\hat{\mathbf{R}}$ are the measurement sensitivity and measurement noise matrices respectively. The matrices $\mathbf{A}$ are $\mathbf{B}$ map the effects of the measurements and their associated noise to the navigation state dispersions.

The correction equations for $\mathbf{C}$ and $\hat{\mathbf{P}}$ at a maneuver time t_m are

$$\mathbf{C}^{+}(t_m) = \mathbf{M}\mathbf{C}^{-}(t_m)\mathbf{M}^T + \mathbf{N}\boldsymbol{Q}_w^{act}\mathbf{N}^T \tag{13}$$

$$\hat{\mathbf{P}}^{+}(t_m) = \left[\hat{\mathbf{I}} + \hat{\mathbf{M}}\right]\hat{\mathbf{P}}^{-}(t_m)\left[I + \hat{\mathbf{M}}\right]^T + \hat{\mathbf{N}}\hat{\mathbf{Q}}_w^{act}\hat{\mathbf{N}}^T \tag{14}$$

The matrices $\mathbf{M}$ and $\hat{\mathbf{M}}$ contain the control partials associated with a linearized two-impulse targeting algorithm. The matrices $\mathbf{N}$ and $\hat{\mathbf{N}}$ are used to map the effects of actuator noise, described by $\boldsymbol{Q}_w^{act}$ and $\hat{\mathbf{Q}}_w^{act}$, into $\mathbf{C}$ and $\hat{\mathbf{P}}$.

LinCov Analysis Setup For this application, the true state is comprised of the inertial position and velocity of the spacecraft and a target vehicle, as well as exponentially correlated random variables (ECRVs, also known as 1st-order Markov processes) that represent the true attitude dispersion, maneuver execution errors (scale factor, misalignment, and bias), star camera misalignment, optical navigation (OpNav) pointing errors and measurement biases. The navigation state contains the same elements as the true state except for maneuver execution errors. This LinCov analysis also incorporates the effect of noise on measurements, maneuvers, and environment models; however, noise is not considered a state variable. The performance specifications for the initiate condition uncertainties of the truth and navigation states along with the inputs characterizing the error models for the measurements and maneuvers and other operational assumptions are referenced in tables listed in the Appendix.

The OpNav measurements consist of the apparent centroid location and apparent angular diameter of a target celestial body. OpNav measurement errors are modeled as a combination of a bias (modeled as an ECRV) and noise. Star tracker measurement errors are modeled as a misalignment (modeled as an ECRV) and noise. The specific camera parameters used in this analysis are not given as this information is currently proprietary.

Thruster errors are modeled as a combination of a misalignment, scale factor, bias, and noise. The misalignment, scale factor, and bias are modeled as ECRVs. These error sources contribute to errors in the delta-v vectors which represent impulsive maneuvers. Table 1 lists each error model component and its corresponding value for the reaction control system (RCS) and main thrusters. It is assumed that RCS thrusters are used for trajectory correction burns while the main thrusters are used for the nominal maneuvers which occur at TLI, outbound powered flyby (OPF), and NRI.

Table 2 lists the initial dispersions and navigation errors for the vehicle's translational and rotational states. Position and velocity uncertainties are expressed in a UVW reference frame, where the U-axis points in the radial direction, V-axis points in the downrange direction, and W-axis points in the crossrange direction (analogous to a local vertical, local horizontal frame). The initial dispersions are amplified by errors in the TLI maneuver. As a correction procedure, a fixed trim burn is performed immediately after TLI. The time of this maneuver is not considered in the optimization process.

Table 3 describes various operational constraints and assumptions. The OpNav measurement pass duration is notionally 2 hours long. However, this duration has lower priority than the constraint on the time between the last OpNav measurement and a maneuver. In the process of searching for an optimal solution, if consecutive maneuvers are placed less than 2 hours apart, then the measurement pass is reduced to ensure the 30 minute gap is enforced. Likewise, maneuvers are constrained to occur at least 30 minutes apart. In the event where maneuvers are separated by exactly 30 minutes, no measurements are taken in between them. The OpNav FOV constraint value is dependent on

camera properties. If the apparent angular diameter of the target celestial body exceeds the field-of-view (FOV) constraint, no OpNav measurements are taken.

Optimization Problem Formulation

The optimization problem formulation for this analysis utilizes two key metrics; the standard deviations of the dispersions on delta-v, $\sigma_{\delta\Delta v}$, and the final relative position, $\sigma_{\delta r}$. Both of these quantities are extracted from the dispersion covariance, $\mathbf{C}$. There is an inherent trade between minimizing the total delta-v dispersions and the final relative position dispersions. As a result, two optimization problems are formulated that compliment one another but capture two distinct yet related objectives. They are referred to as Problem #1 and Problem #2.

The Problem #1 objective minimizes the total delta-v dispersion across all midcourse correction maneuvers subject to a constraint on the relative position dispersion at the final time. The relative position dispersion constraint is implemented as a penalty function. When the constraint is violated, a large constant κ is added to the value of the objective function.

$$\text{Problem } \#1: \ \text{minimize} \ \sum_{m=1}^{N} \sigma_{\delta\Delta v}(t_m) + \kappa \,\text{sgn}\big(\max(0, \sigma_{\delta r}(t_f) - \sigma_{\delta r}^{req})\big) \tag{15}$$

The Problem #2 objective minimizes the relative position dispersion at the final time subject to a constraint on the total delta-v dispersion across all midcourse correction maneuvers. Like Problem 1, the delta-v dispersion constraint is implemented as a penalty function.

$$\text{Problem } \#2: \ \text{minimize} \ \sigma_{\delta r}(t_f) + \kappa \,\text{sgn}\big(\max(0, \sum_{m=1}^{N} \sigma_{\delta\Delta v}(t_m) - \sigma_{\delta\Delta v}^{req})\big) \tag{16}$$

Due to their complex nature, both optimization problems are solved using a GA. During each GA iteration, candidate values of the optimization variables are passed to the LinCov simulation, which is then evaluated to determine the values of the cost and penalty functions. This process is shown in Figure 4.

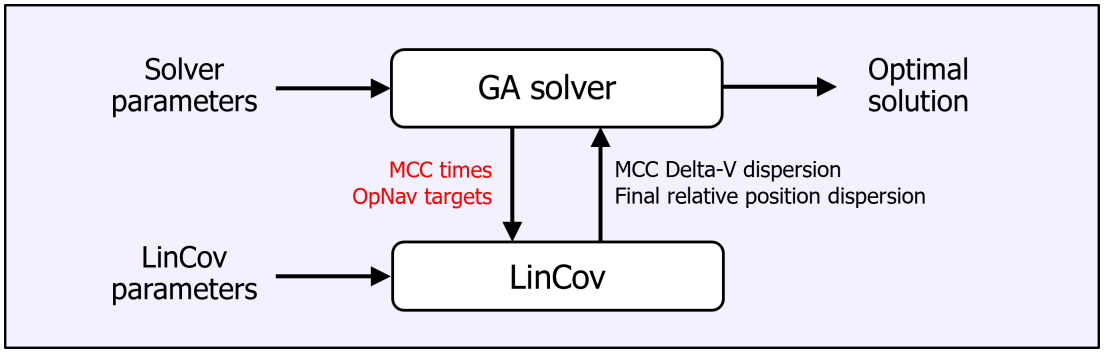

Figure 4. Functional relationship between the LinCov simulation and GA solver.

The GA refines its search for an optimal solution through a process inspired by natural selection.[14] Each generation of new candidate solutions is influenced by the performance of candidate solutions from previous iterations. Ultimately this process provides a way of efficiently searching for a global optimal solution.

GN&C RPOD PERFORMANCE ANALYSIS

To motivate the robust trajectory optimization techniques for rendezvous in an NRHO, a scenario is adopted that starts with the trans-lunar injection (TLI) burn. Upon arrival at the moon, the spacecraft executes the outbound power flyby (OPF) burn to strategically enter the NRHO near a target vehicle. Several potential outbound trajectory correction (OTC) burns are alloted prior to the NRHO insertion (NRI) point that target a specific offset to the target vehicle. For the following rendezvous scenarios, this offset is 300 km along the docking axis. The translational burn used to insert into the NRHO is referenced as the NRI burn.

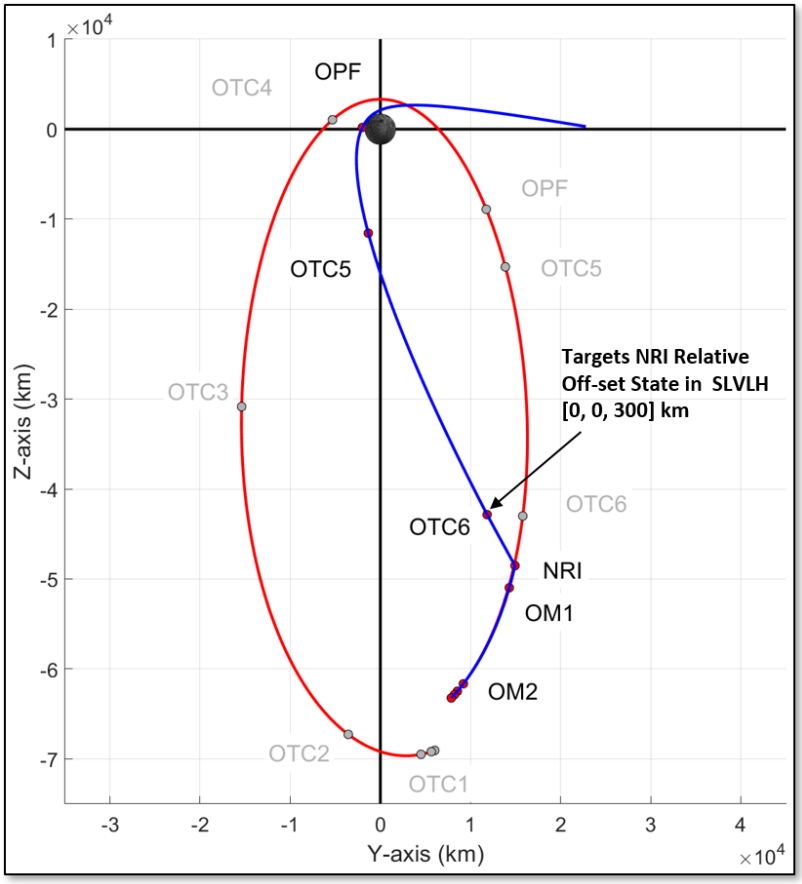

Figure 5. Simulated cis-lunar trajectory with baseline trajectory correction burn locations

The trajectory profiles for both vehicles in the Earth-Moon Rotating frame are shown in Figure 5. The solid red line highlights the target vehicle's NRHO orbit and the solid blue line represents the chaser spacecraft inserting into the NRHO. The solid red and gray dots indicate the location of each vehicle at different epochs (such as major burns) during the flight.

Once the chaser spacecraft has successfully entered the NRHO, it initiates a series of maneuvers to rendezvous within 30 km of the target vehicle at the NRHO rendezvous (NRR) point. These orbit maintenance (OM) burns target specific relative locations to the target vehicle that are labeled as the OM1 and OM2 burns. The relative motion in the sun-reference local vertical local horizontal (S-LVLH) frame is shown in the plots in Figure 6. Figure 6(a) emphasizes the relative motion

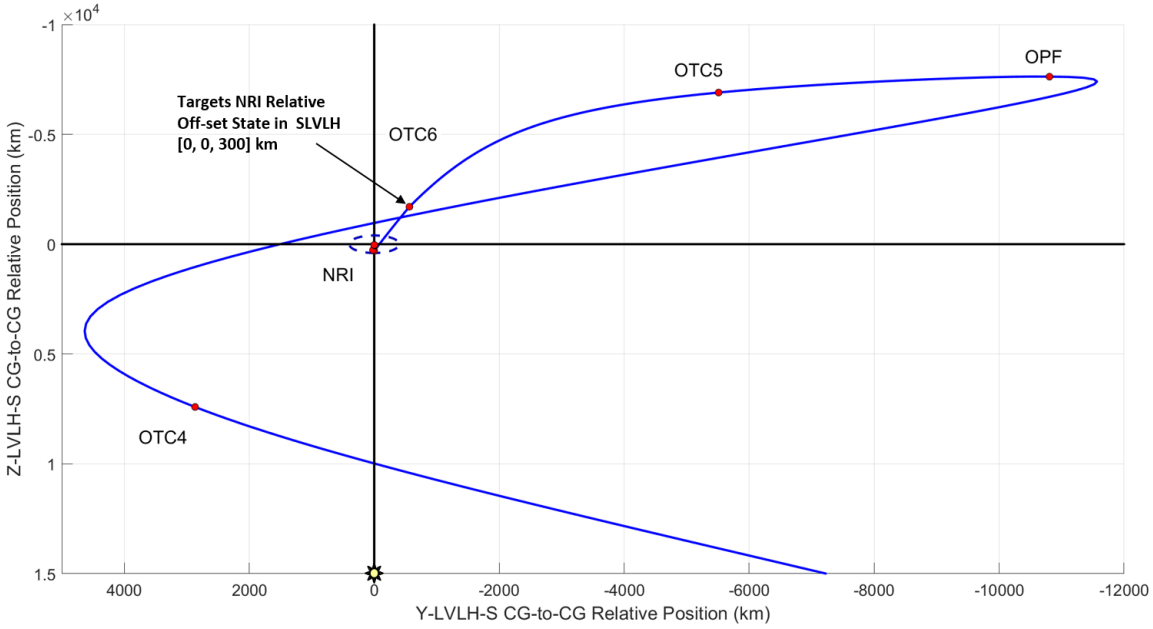

(a) Relative Motion Prior to NRHO Insertion

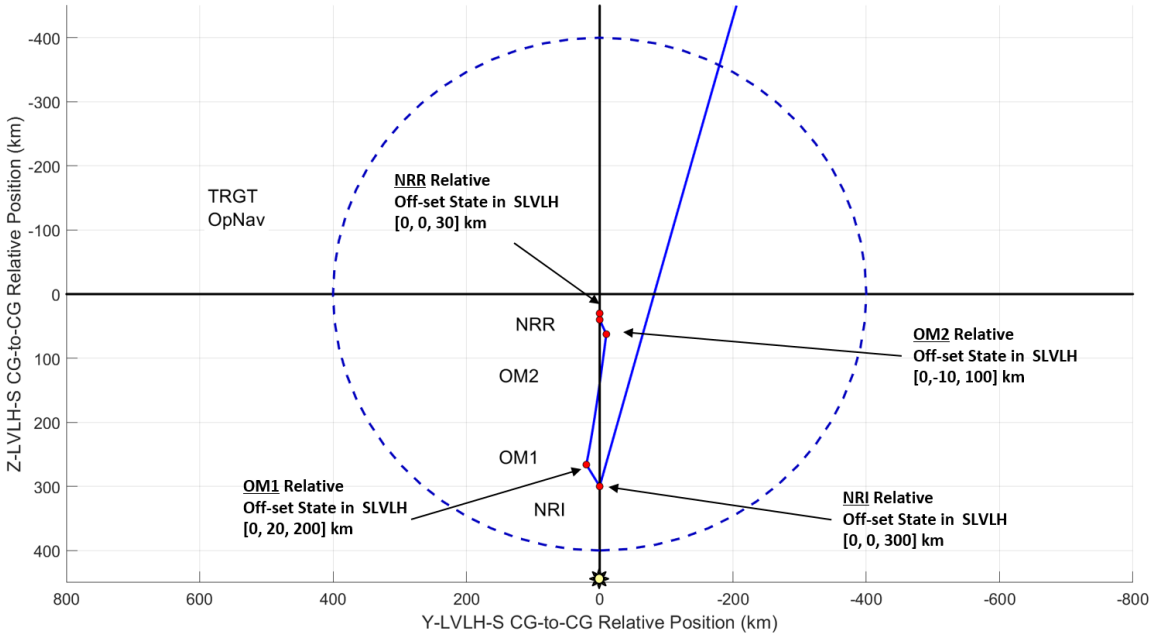

(b) Relative Motion After NRHO Insertion

Figure 6. Simulated relative motion trajectory with baseline trajectory correction burn locations

prior to NRHO insertion and Figure 6(b) highlights the *straight line* relative motion after NRHO insertion. The targeted dashed circle indicates the range at which optical bearing measurements to the target vehicle are available. Initially, four scenarios are evaluated to illustrate the dependency and trade off between sensor utilization and the trajectory profile as depicted in Figure 7. The trends and sensitivity from these simple examples are then extended to derive optimal trajectory correction

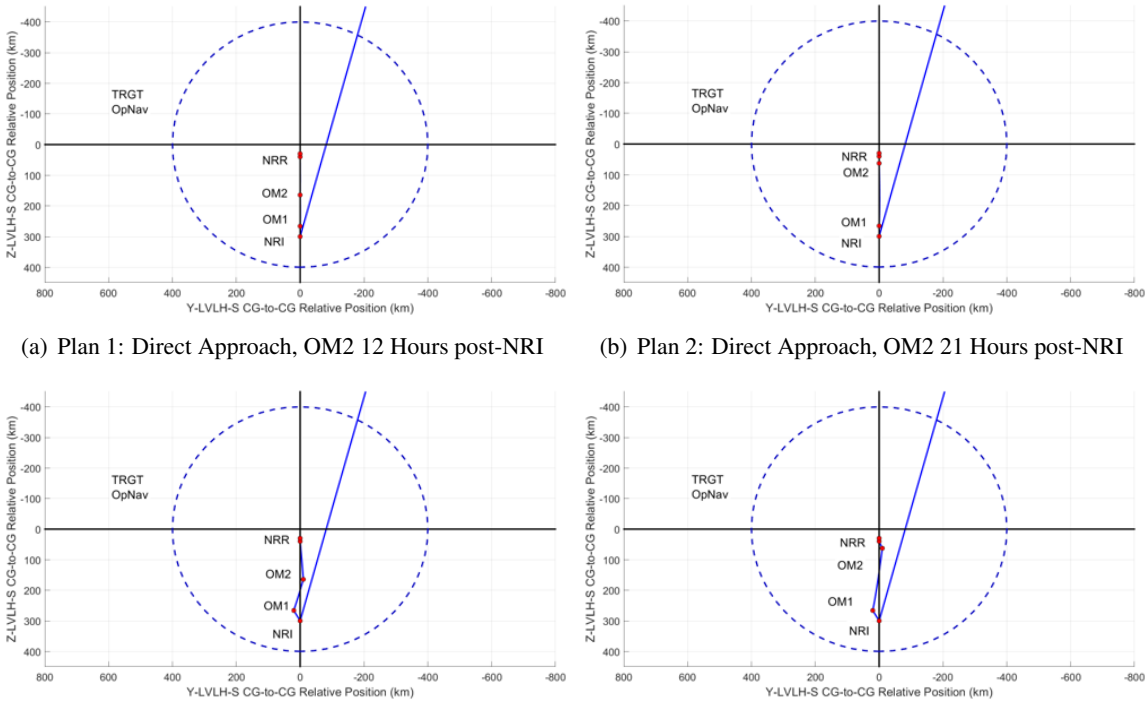

(a) Plan 1: Direct Approach, OM2 12 Hours post-NRI (b) Plan 2: Direct Approach, OM2 21 Hours post-NRI

(c) Plan 3: Observable Approach, OM2 12 Hours post-NRI (d) Plan 4: Observable Approach, OM2 21 Hours post-NRI

Figure 7. Various Rendezvous Profiles with Different Orbit Maintenance Burns

burns.

Results

For each of these four rendezvous trajectory profiles, they are evaluated with the following relative sensors: 1) no relative sensors, 2) angles to target vehicle (line-of-sight to the target), and 3) angles to the target along with range and range-rate measurements. The sensor accuracies and other analysis performance specifications are provided in the Appendix. Figure 8 highlights the relative trajectory dispersions for the cases when no relative sensors are used and when angles-only measurements are available to the target vehicle.

To initiate the NRR burn for proximity operations, it is notionally required to have the relative position dispersions less than 3.5 km (3-sigma). Figure 9 provides a summary of the different scenarios that satisfied the NRR position requirement (green) and which ones failed (red). It is clear from this illustrative example that depending on the trajectory profile selected and the available sensors, the dispersion requirements for initiating the NRHO rendezvous (NRR) burn are satisfied while others are not. The question remains, what is optimal location for the orbit maintenance (OM) burns that reduce total delta-v usage (nominal plus 3-sigma dispersions) while satisfying the NRR relative position and velocity dispersion constraints. Or, what are the optimal translational burn locations that reduce the NRR position dispersions while satisfying a maximum limit of total delta-v usage. The following section will now extend this illustrative example to be more comprehensive robust trajectory optimization problem.

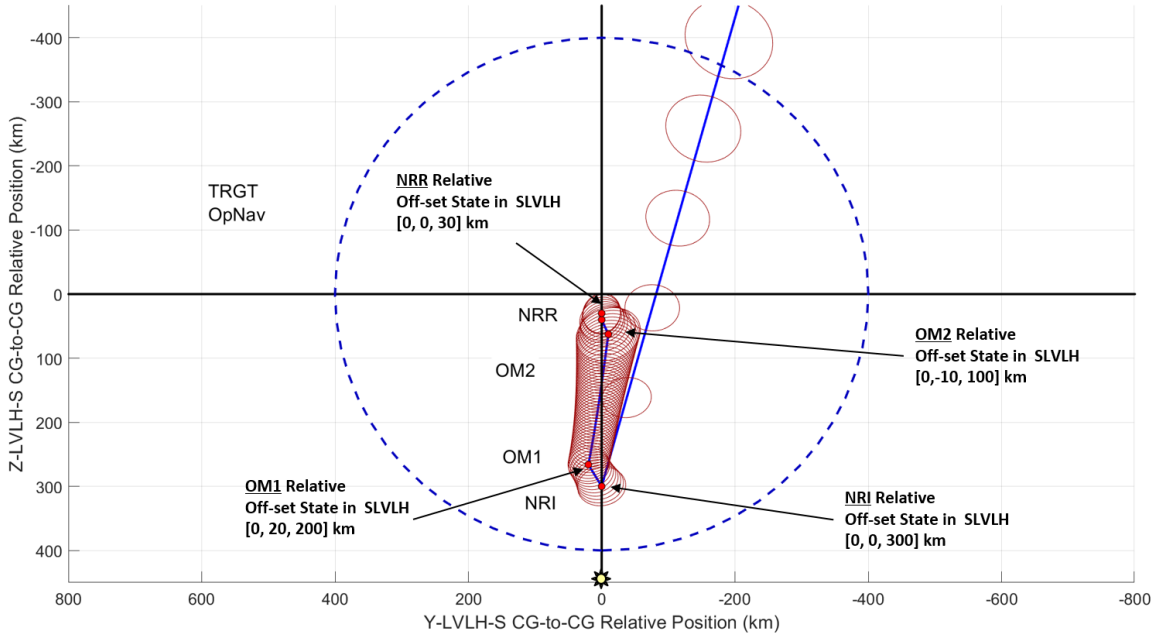

(a) No Relative Sensors

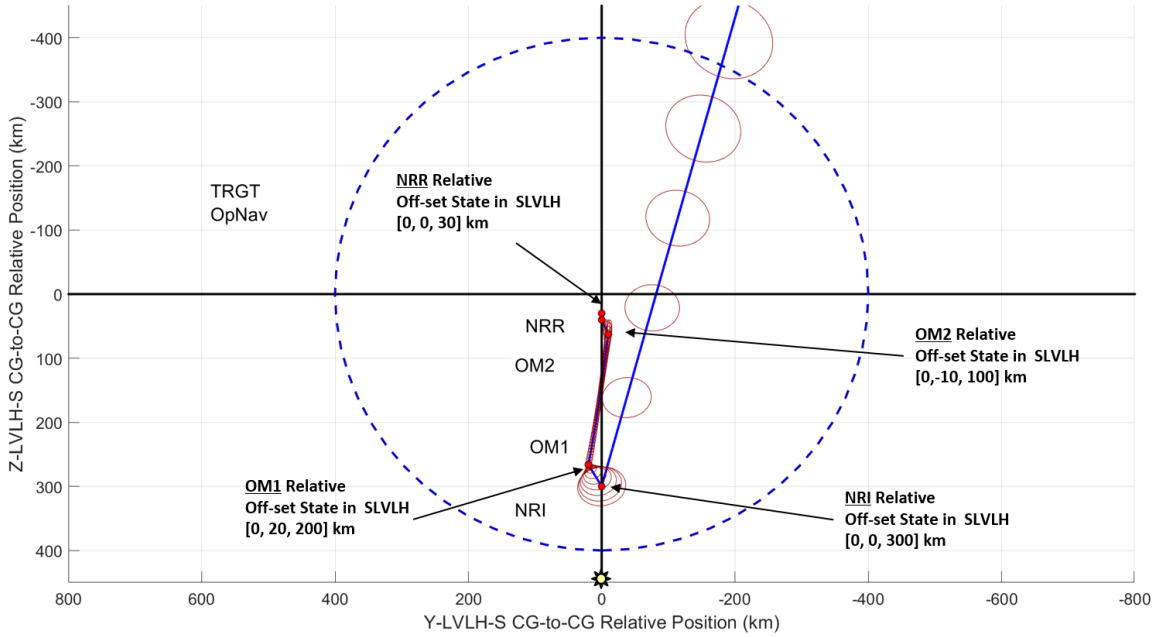

(b) Relative Angle Measurements to Target

Figure 8. Simulated relative motion trajectory dispersions with baseline trajectory correction burn locations

RENDEZVOUS ROBUST TRAJECTORY OPTIMIZATION ANALYSIS

In this section the new robust trajectory design technique is used to determine the optimal trajectory correction burn locations and OpNav viewing targets for a complete end-to-end mission

Relative Sensors	Relative Burn Plan			
	Plan 1: Direct	Plan 2: Direct	Plan 3: Observable	Plan 4: Observable
Suite 1: No Relative Sensors	Case 1	Case 2	Case 3	Case 4
Suite 2: Angles Only	Case 5	Case 6	Case 7	Case 8
Suite 3: Angles and Range/Rate	Case 9	Case 10	Case 11	Case 12

Green = 3-sigma relative NRR dispersions are within the requirement
Red = 3-sigma relative NRR dispersions are significantly outside the requirement by more than 2km
Orange 3-sigma relative NRR dispersions are outside the requirement by less than 2km

Figure 9. NRHO Rendezvous Insertion Performance Summary

spanning from trans-lunar injection (TLI) to NRR. For this scenario the *direct approach* relative motion profile is adopted following NRHO insertion with *Plan 1* burn schedule as the baseline where OM2 occurs 12 hours post-NRI as summarized in Figure 7(a). These notional baseline trajectory correction burn placements from TLI to NRR are highlighted in Figure 10. The non-optimal baseline results based on a two-camera system are presented first followed by the optimal solutions to Problem #1 and Problem #2 that utilize a single camera and have objective functions to minimize delta-v and final position dispersions respectively.

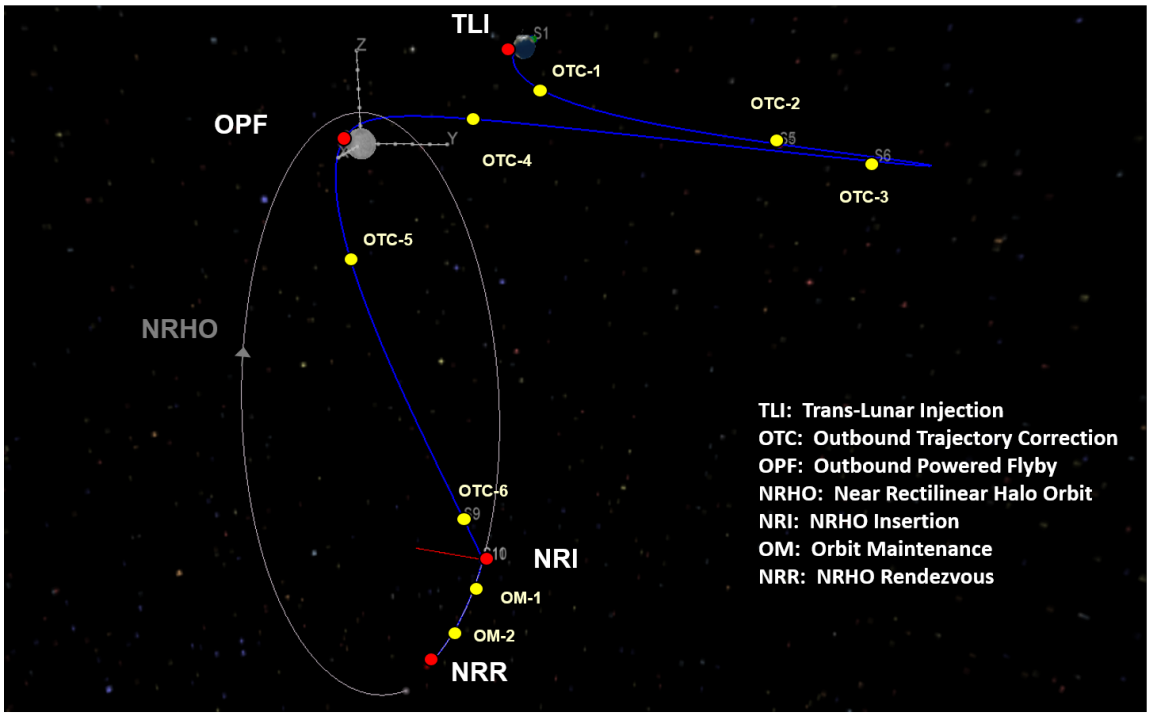

Figure 10. TLI to NRHO Trajectory Profile and Baseline Trajectory Correction Burn Placement.

Baseline Results

The relative position dispersion time history, OpNav scheduling, relative position estimation error time history, and trajectory correction delta-v dispersions using the baseline trajectory correction

burn locations with a two-camera OpNav system are provided in Figure 11. The vertical lines denote maneuver locations; solid lines indicate nominal translational burns and dashed lines indicate the trajectory correction burns.

The two-camera OpNav system assumes that measurements of the Earth, Moon, and target vehicle can be taken simultaneously. However, due to camera FOV and range constraints, there are instances where measurements cannot be taken. This is shown on the OpNav schedule plot. The

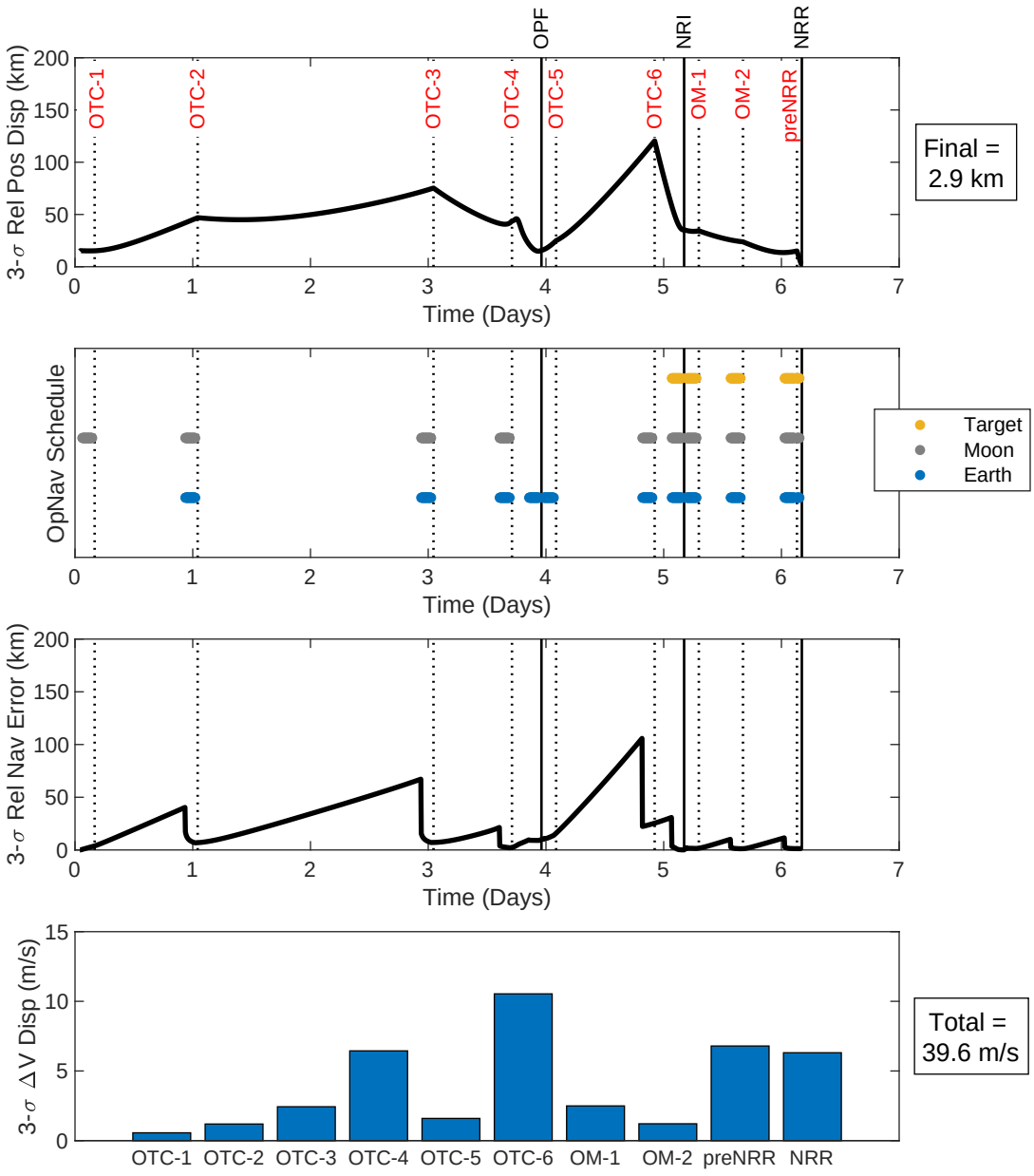

Figure 11. BASELINE RESULTS: Relative position dispersion time history, OpNav scheduling, relative position estimation error time history, and trajectory correction delta-v dispersions using the baseline locations and two-camera OpNav system.

FOV constraint is violated as the vehicle remains close to the Earth before the first outbound trajectory correction (OTC-1) and as it passes near the Moon around the time of OPF. The target vehicle is too distant for viewing until the measurement pass preceding NRI.

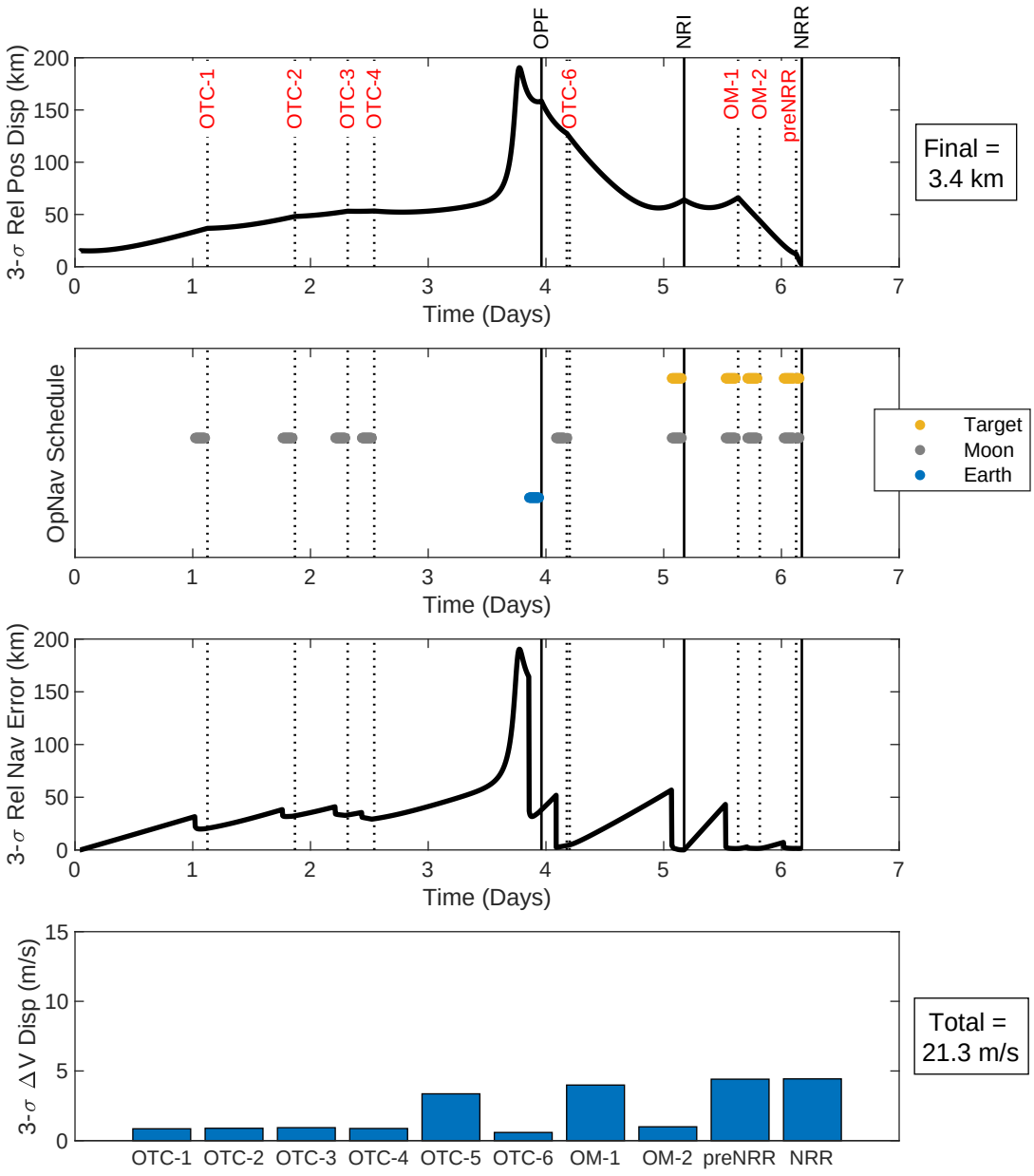

Figure 12. PROBLEM #1 RESULTS: Relative position dispersion time history, OpNav scheduling, relative position estimation error time history, and trajectory correction delta-v dispersions for the optimal solution to problem 1.

Problem #1: Minimize Delta-v Dispersion

The objective function for this problem formulation is to determine the translational correction burn times and OpNav viewing targets which minimize the total trajectory correction burn delta-v dispersions while ensuring the final relative position dispersions do not exceed the notional requirement limit of 3.5 km. There are 9 trajectory corrections scheduled, and their grouping is consistent with the baseline setup: 4 between TLI and OPF, 2 between OPF and NRI, and 3 between NRI and

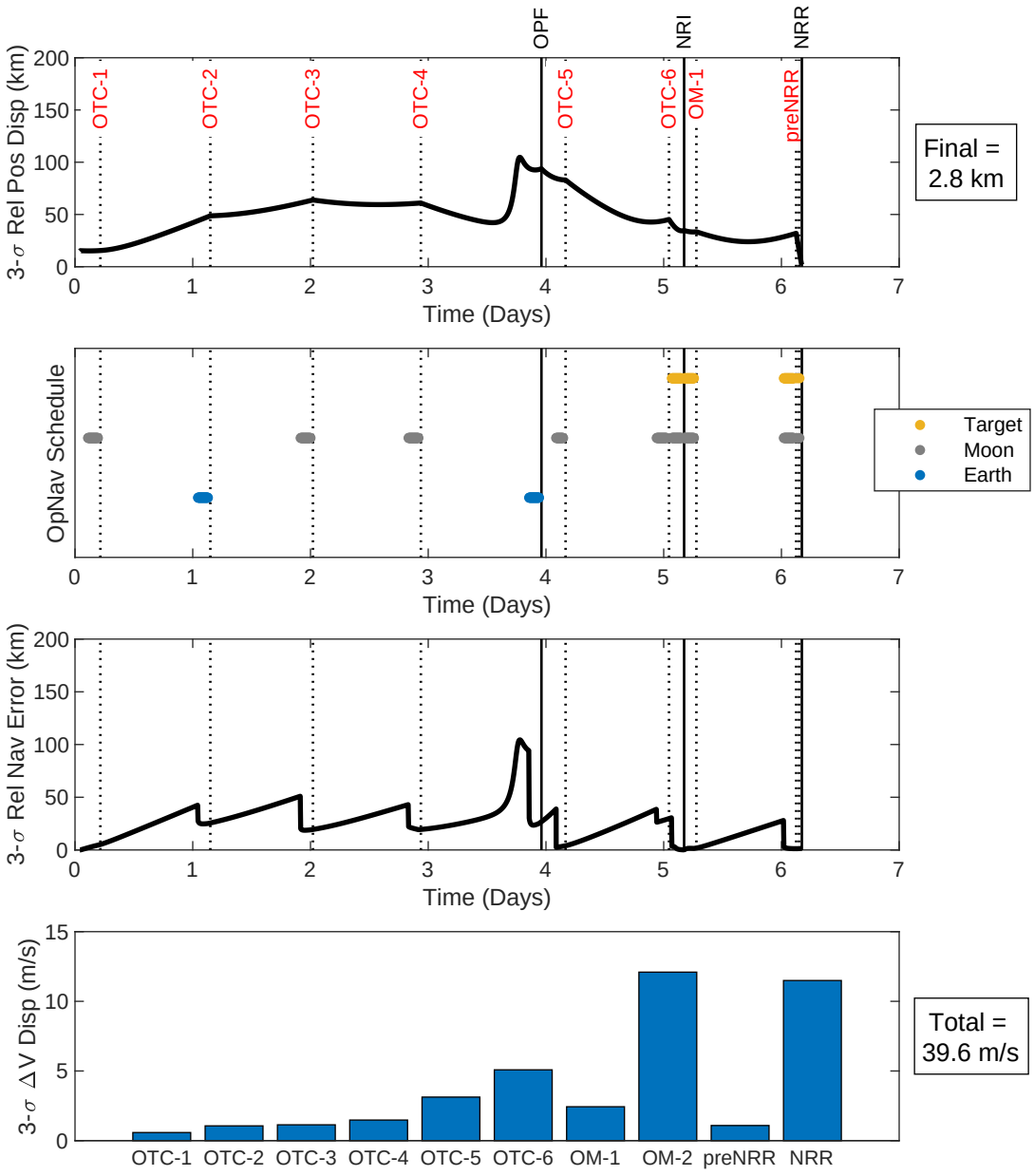

Figure 13. PROBLEM #2 RESULTS: Relative position dispersion time history, OpNav scheduling, relative position estimation error time history, and trajectory correction delta-v dispersions for the optimal solution to problem 2.

NRR. Figure 12 shows the resulting relative position dispersion time history, OpNav scheduling, relative position estimation error time history, and trajectory correction delta-v dispersions.

There is a noticeable shift in the trajectory correction burns location from the baseline. OTC-1 through OTC-4 are more tightly grouped, spanning only 1.5 days. This arrangement leads to a drop in the delta-v dispersions associated with OTC-3 and OTC-4. OTC-5 occurs slightly later to allow for enough separation from the Moon for OpNav measurements to be taken. As a result, the targeting accuracy is improved and the relative position dispersion decreases. OTC-6 occurs almost immediately after OTC-5 which decreases its delta-v dispersion. OM-1 and OM-2 occur later resulting in less corrective effort at pre-NRR and in turn a lower delta-v dispersion. Overall, these results show that through optimally selecting the trajectory correction burn times and OpNav viewing target, the 3.5 km relative position dispersion requirement can be met with a single-camera OpNav system while also reducing the overall delta-v dispersion.

Problem #2: Minimize Relative Position Dispersion

The objective of this problem formulation is to determine the trajectory correction burn times and OpNav viewing targets which minimize the final relative position dispersion while ensuring the total trajectory correction delta-v dispersion does not exceed 39.6 m/s, the valued obtained during the baseline scenario. There are 9 trajectory correction burns scheduled, and their grouping is consistent with the baseline setup. Figure 13 shows the resulting relative position dispersion time history, OpNav scheduling, relative position estimation error time history, and trajectory correction delta-v dispersions.

Similar to Figure 12, there is a noticeable shift in the trajectory correction burn placement from the baseline locations. OTC-3 and OTC-4 occur early enough to reduce delta-v dispersions yet late enough to maintain a reasonable level of relative position dispersion and estimation error. Similar to Figure 12, OTC-5 occurs slightly later to allow for Moon OpNav measurements, resulting in a lower relative position dispersion before OTC-6. OM-2, preNRR, and NRR occur almost immediately after one another to reduce the final relative position dispersion. As a result, the delta-v dispersions associated with OM-2 and NRR increase, but not enough to violate the delta-v dispersion constraint. Overall, these results show that through optimally selecting the trajectory correction burn times and OpNav viewing target, the baseline trajectory correction delta-v dispersion can be met with a single-camera OpNav system while also reducing the final relative position dispersion.

CONCLUSION

The development of robust trajectory optimization where linear covariance techniques are integrated with optimization algorithms to maximizes system performance is emerging as a key technology for lunar exploration and beyond. By having the trajectory design process account for system uncertainty early in the design cycle or onboard a spacecraft, it can improve performance and provide significant cost savings or redesign efforts. Although these concepts have been applied and are being applied to a variety of space flight applications, this paper addresses the emerging demands of performing rendezvous in a near rectilinear halo orbit. After doing an initial sensitivity study to show the interdependence between various navigation sensor suites and different relative trajectory profiles, it became evident that optimal performance identified a favorable combinations of trajectory design attributes with selected navigation targets. These insights were then extended to demonstrate the optimal placement of trajectory correction burns and optical navigation targets

in an end-to-end scenario starting from a trans-lunar injection burn through the initiating of close proximity operations for rendezvous and docking in an NRHO.

REFERENCES

[1] K. Hambleton, "Deep Space Gateway to Open Opportunities for Distant Destinations," *NASA*, 28 Mar 2017.

[2] J. Williams, D. E. Lee, R. J. Whitley, K. A. Bokelmann, D. C. Davis, and C. F. Berry, "Targeting Cislunar Near Rectilinear Halo Orbits for Human Space Exploration," *American Astronautical Society*, 1017, pp. AAS 17–267.

[3] D. J. Grebow, M. T. Ozimek, K. C. Howell, and D. C. Folta, "Multibody Orbit Architectures for Lunar South Pole Coverage," *Journal of Spacecraft and Rockets*, Vol. 45, No. 2, March-April 2008.

[4] K. Jin, D. K. Geller, and J. Luo, "Robust Trajectory Design for Rendezvous and Proximity Operations with Uncertainties," *Journal of Guidance, Control, and Dynamics*, Vol. 43, No. 4, 2020, pp. 741–753.

[5] D. K. Geller, S. Shuster, D. Woffinden, and S. Bieniawski, "Robust Cislunar Trajectory Optimization via Midcourse Correction and Optical Navigation Scheduling," *44th Annual AAS Guidance, Navigaiton and Control Conference*, Breckenridge, CO, AAS 22-065, 4-9 February 2022 2022.

[6] G. Calkins, D. Woffinden, and Z. Putnam, "Robust Trajectory Optimization for Guided Powered Descent and Landing," *2022 AAS/AIAA Astrodynamics Specialist Conference*, Charlotte, NC, AAS 22-660, 7-11 August 2022 2022.

[7] J. Joshi, D. Woffinden, and Z. Putnam, "End-to-End Mars Aerocapture Analysis Using Linear Covariance Techniques and Robust Trajectory Optimization," *2022 AAS/AIAA Astrodynamics Specialist Conference*, Charlotte, NC, AAS 22-678, 7-11 August 2022 2022.

[8] P. S. Maybeck, *Stochastic models, estimation, and control*, Vol. 1. New York: Academic Press, 1979.

[9] D. K. Geller, "Linear Covariance Techniques for Orbital Rendezvous Analysis and Autonomous Onboard Mission Planning," *Journal of Guidance, Control, and Dynamics*, Vol. 29, November-December 2006, pp. 1404–1414.

[10] T. J. Moesser and D. K. Geller, "Guidance and Navigation Linear Covariance Analysis for Lunar Powered Descent," *AAS/AIAA Astrodynamics Specialist Conference*, Mackinac Island, Michigan, AAS 07-313, 19-23 August 2007.

[11] D. Geller and D. Christensen, "Linear Covariance Analysis for Powered Lunar Descent and Landing," *The Journal of Spacecraft and Rockets*, Vol. 46, Nov-Dec 2009, pp. 1231–1248.

[12] D. Woffinden, S. Robinson, J. Williams, and Z. Putnam, "Linear Covariance Analysis Techniques to Generate Navigation and Sensor Requirements for the Safe and Precise Landing - Integrated Capabilities Evolution (SPLICE) Project," *AIAA Scitech 2019 Forum*, San Diego, CA, AIAA 2019-0662, 7-11 January 2019 2019.

[13] J. W. Williams, W. E. Brandenburg, D. C. Woffinden, and Z. R. Putnam, "Validation of Linear Covariance Techniques for Mars Entry, Descent, and Landing Guidance and Navigaiton Performance Analysis," *AIAA Scitech 2022 Forum*, 2022, 10.2514/6.2020-0597.

[14] J. C. Spall, "Stochastic Optimization," *Handbook of Computational Statistics: Concepts and Methods* (J. Gentle, W. Hardle, and Y. Mori, eds.), ch. 7, pp. 173–201, Springer-Verlag, Heidelberg, 2 ed., 2012.

APPENDIX

Tables 1, 2, and 3 list relevant LinCov parameters and operational constraints used in the robust trajectory optimization analysis.

Table 1. Error sources and values for RCS and main thrusters used in the end-to-end analysis.

Description	Value		Units
	RCS Thrusters	Main Thrusters	
Misalignment steady-state (3-σ)	30	4.5	mrad
Misalignment time constant	2.78	2.78	hr
Scale factor steady-state (3-σ)	3	0.45	%
Scale factor time constant	2.78	2.78	hr
Bias steady-state (3-σ)	225	600	mm/s
Bias time constant	2.78	2.78	hr
Noise (3-σ)	225	600	mm/s

Table 2. Initial dispersions and navigation errors used in the end-to-end analysis.

Description	Value (3-σ)	Units
Position dispersion (U,V,W)	(10, 20, 20)	km
Velocity dispersion (U,V,W)	(15, 6, 5)	m/s
Attitude dispersion (per axis)	0.5	deg
Position estimation error (U,V,W)	(50, 50, 50)	m
Velocity estimation error (U,V,W)	(0.05, 0.05, 0.05)	m/s
Attitude estimation error (per axis)	0.15	deg

Table 3. Operational constraints and assumptions used in the end-to-end analysis.

Description	Value	Units
Notional OpNav measurement pass duration	2	hr
Time between last OpNav measurement and maneuver	30	min
Minimum time between maneuvers	30	min
OpNav measurement frequency	60	sec
OpNav FOV constraint	16	deg